Effect of intravascular bubbles on perfusate flow and gas elimination rates following simulated decompression of a model tissue

A. BAZ and S. I. ABDEL-KHALIK

Mechanical Engineering Dept., The Catholic University of America, Washington, DC; and Nuclear Engineering Dept., University of Wisconsin, Madison, WI

Baz A, Abdel-Khalik SI. Effect of intravascular bubbles on perfusate flow and gas elimination rates following simulated decompression of a model tissue. Undersea Biomed Res 1986;13(1):27–44.—This study deals with the monitoring of the elimination rates of gases from a porous cylindrical model of the human tissue during simulated single-stop decompression schedules. The data suggest the presence of an optimal decompression stop for each dive at which the gas elimination rate is maximum. The effect of varying the flow rate and the viscosity of the liquid perfusing the tissue model on the elimination rate is determined for different diving conditions. Although this study has been carried out on a single tissue model, it provides means for explaining some of the physiological phenomena observed in human tissues.

intravascular bubbles
optimal elimination rates
optimal decompression stop

The presence of inert gas bubbles during asymptomatic decompression is a well proven and accepted phenomenon in diving as reported, for example, in the comprehensive account of Weathersby and Homer (1). Extensive efforts have been exerted recently to study this phenomenon in an attempt to understand the basic principles involved in bubble formation (2–6), and bubble growth (7–8), as well as bubble transport characteristics (9–11). Such efforts aim eventually at developing an alternate bubble theory of decompression to replace the empirical, but practically safe, Haldanian theory which is based on premises that violate the bubble-presence phenomenon (12–14).

Most of the current bubble studies have emphasized the effect of the various conventional decompression practices on the bubble formation, growth, and stability in order to define surfacing criteria that would limit the growth of the developed bubbles (3–6). Furthermore, these studies have dealt primarily with the phenomena associated with extravascular and/or stationary bubbles either in vivo tissues (9) or in various tissue models such as gelatins (4–6) and rubber (8). Few bubble studies

have, however, attempted to correlate the effect of intravascular bubbles on the gas elimination rate (7, 14), although such bubbles have been detected by their direct (15–16) or indirect (17–19) physiological effects.

Due to such well proven effects, this study was conducted to develop an understanding of the influence of intravascular bubbles on the decompression mechanism in general, as well as on the elimination rate and the pressure transients in the tissue model and the liquid perfusing it, particularly at different simulated dive conditions.

EXPERIMENTAL FACILITIES, MATERIALS, AND METHODS

This study is based on the tissue-capillary model shown in Fig. 1 where the tissue is simulated by a storage space connected to a porous-hollow cylinder which is perfused internally by a liquid stream. Such a model, called the Krogh cylinder model (20), has been accepted in the simulation of inert gas transport during decompression (21–22).

The tissue-capillary model was installed as shown in Fig. 2 where it was subjected to different levels of tissue initial pressures, liquid back pressure, and liquid flow rates as well as liquid viscosities.

A. The experimental setup

The experimental setup incorporates two main sections which are:

1. Compressed gas section (Fig. 2). In this section, the pressure of the compressed gas is controlled at the desired level by the pressure regulator *A*. The gas is then allowed to flow into the storage link *C* via the two-position, manually operated valve *B*. The pressure of the gas inside the tank is monitored by the pressure gauge *D* until the present level is attained and valve *B* is then closed.

The compressed gas, at that preset initial level, is allowed to flow through the tissue model by energizing the two-position solenoid valve *E*. The released gas will pass through the pores of the tissue into the liquid stream where it is carried to the liquid reservoir. The solenoid valve is then deenergized when the storage tank pressure becomes equal to the liquid pressure.

The compressed gas section also incorporates a branch that has a pressure regulator *F*, a pressure gauge *G*, and a two-position solenoid valve *H*. These components provide means for cleaning the tissue model after every test in order to maintain it in an unplugged condition. Furthermore, the pressure of the flushing branch is controlled to equalize the liquid pressure in order to prevent liquid from flowing into the gas section, particularly during the process of filling the storage tanks.

2. Liquid section (Fig. 2). In the liquid section, a positive displacement pump *I* is used to circulate the liquid through the tissue model at flow rates controlled by the pump speed and at a pressure regulated by the valve *L*. The liquid flow rate is monitored by the flow meter *J* while its pressure is measured by the pressure gauge *K*.

The pump is a positive displacement type because it is characterized by its ability of pumping fluids at constant flow rates irrespective of the level of the delivery

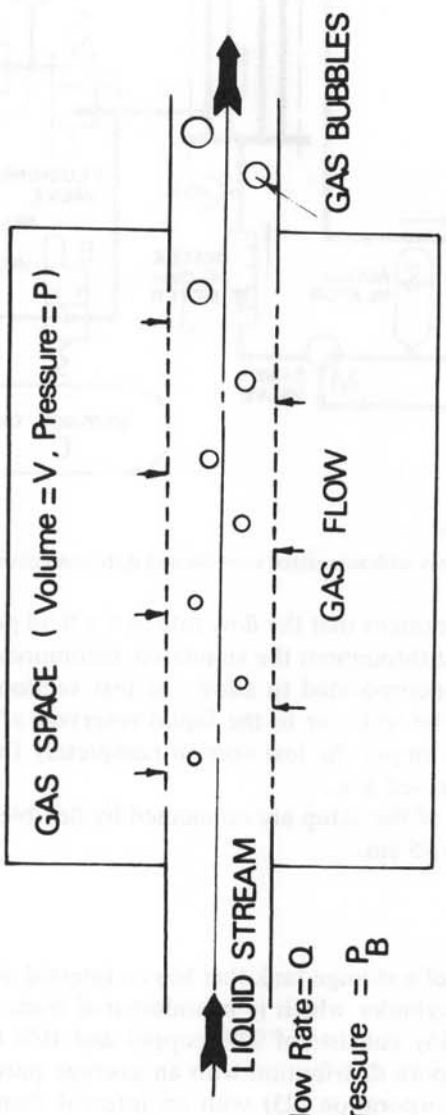

Fig. 1. A typical tissue-capillary arrangement.

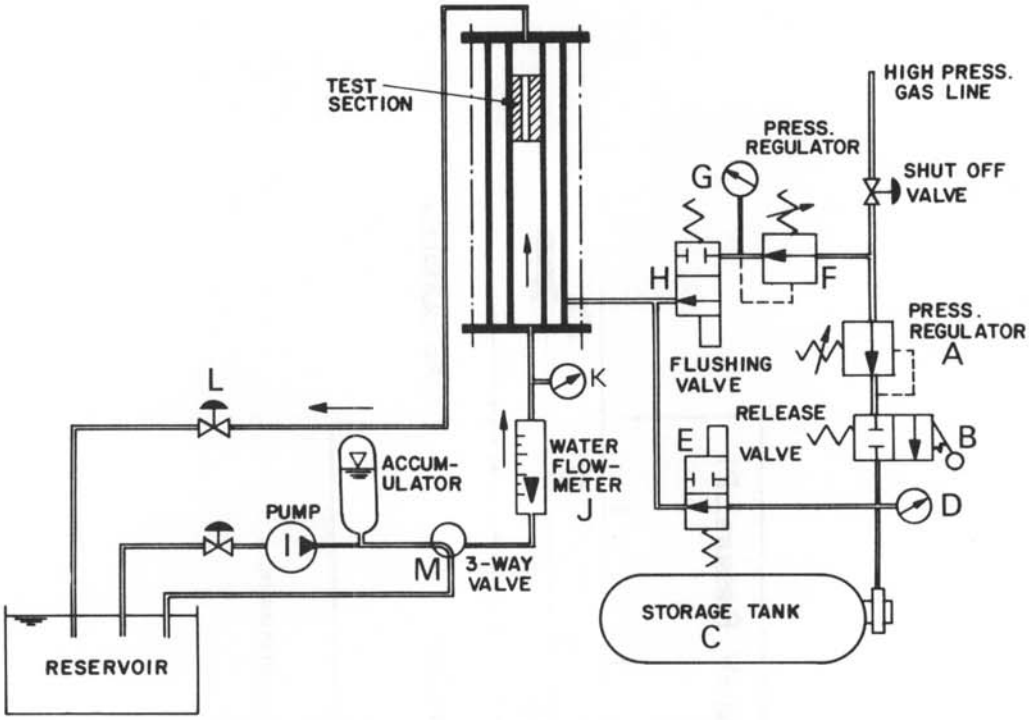

Fig. 2. Schematic of the apparatus with associated controls and instrumentations.

pressure. Such a feature guarantees that the flow rate of the fluid perfusing the tissue model is maintained constant throughout the simulated decompression process.

A three-way valve *M* is incorporated to allow the test section to be connected either to the pump, during the tests, or to the liquid reservoir after the tests have been carried out in order to empty the test section completely from the liquid and flush it properly with compressed gas.

The different components of the setup are connected by flexible tygon tubing that has an internal diameter of 0.95 cm.

B. Tissue model

The tissue model is made of a storage tank that has an internal volume of 8.8 liters (STP) and a porous-hollow cylinder which is manufactured from a sintered bronze alloy type SAE 841. The alloy consists of 90% copper and 10% tin of high purity. The cylinder has a random pore distribution with an average porosity of 17%. It is manufactured by Masten Corporation (23) with an internal diameter of 1.25 cm, external diameter of 2.5 cm, and length of 16.25 cm.

C. Perfusing fluid

The tissue model has been saturated with compressed air and perfused either with water in most of the tests, or with 25% glycerine mixture in the remainder of the runs. Conducting the tests with these two types of fluids was essential to study the

role of viscosity on the simulated intravascular bubbles. Water was selected because it has a viscosity which is nearly equal to that of blood flowing inside 4–7 μm capillaries (24). The 25% glycerine-water mixture was used, however, for two reasons. Others have proven that it simulates closely the flow characteristics of blood in arteries (25). Second, its viscosity is 2.25 times that of water and therefore would simulate the effect of increasing the blood viscosity with reduced dive temperatures. It has been reported that the viscosity increases two- to threefold when the body temperature drops from 37–20°C (26).

D. Methods

The tissue storage space is filled initially with air at a predetermined value to simulate the tissue pressure following a particular dive condition. The pressure of the perfusing fluid is controlled at set values to represent the decompression stop. Air is then released from the gas storage space and is allowed to flow through the porous cylinder into the perfusing liquid stream. Such a process will continue until the gas pressure in the tank decreases to a level where it equilibrates the fluid pressure. During this process of simulated gas elimination, the tissue and liquid pressures are recorded as a function of time. The initial tissue pressure is varied from 1.5–3 ATA while the back pressure assumes values between 1–1.66 ATA giving simulated decompression ratios (i.e., tissue pressure/back pressure) of 1.5–3. Such values are comparable to the ratios experienced in air diving.

Under such dive conditions, the flow rate of the perfusing liquid is varied between 2–8.7 ml/s in the case of water, and between 1.6–12.8 ml/s in the case of the glycerine mixture. With these flow rates, a minimum flow velocity of 1.3 cm/s is attained inside the tissue model which is very close to that encountered in capillary flows (27).

RESULTS

A. Tissue perfused with water

Figure 3*a, b* show the pressure transients recorded in the tissue model and the water stream following decompression of the air-saturated tissue (3 ATA) into water flowing at a rate of 4.1 and 8.7 ml/s, respectively. The water pressure (tissue back pressure) is maintained in the two cases at 1.66 ATA. In other words, the tissue model is subjected to a surfacing schedule with a decompression ratio of 1.80.

It is evident that the tissue gas pressure drops in an exponential fashion whereas the liquid pressure is no longer steady but oscillating in nature.

The phenomenon of liquid pulsation observed during this simulated decompression process emphasizes the importance of the role of intravascular bubbles in controlling the gas elimination rate. In such a phenomenon, the gas bubbles released into the liquid stream result in a sharp rise in the liquid pressure which reduces, in effect, the driving force between the tissue and the liquid. This decreases accordingly the elimination rate. But as the released gas is eliminated by the flowing liquid and disposed of in the liquid reservoir (simulating the diver's lungs), the liquid pressure drops thus increasing again the driving force. More gas bubbles will then be released into the liquid stream producing another rise in liquid pressure until the liquid washes

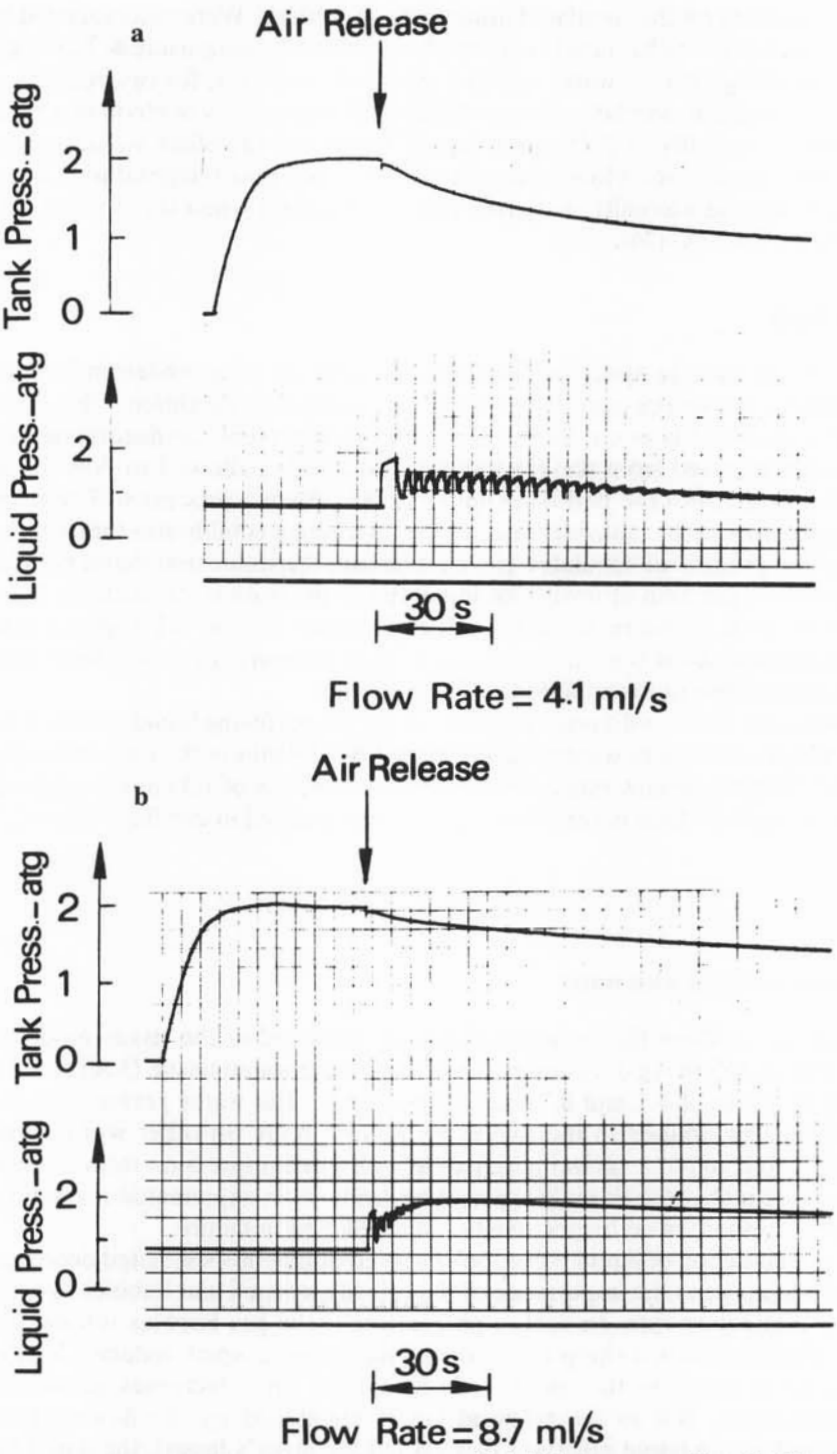

Fig. 3*a:* Time histories of air and water pressures with initial air pressure P_I = 3 ATA, the back pressure P_B = 1.66 ATA and water flow rate = 4.1 ml/s. *b:* Time histories of air and water pressures with initial air pressure P_I = 3 ATA, the back pressure P_B = 1.66 ATA and water flow rate = 8.7 ml/s.

the bubbles away to drop the pressure to its normal value. The cycle of gas release, pressure build-up, elimination impairment, gas wash-out, and improved elimination with subsequent gas release is repeated over a long period of time during the decompression process. This time period, through which the flow pulsations are sustained, depends primarily on the flow rate of the liquid perfusing the tissue such that it is longer for small rates and shorter for larger flow rates as indicated in Fig. 3*a, b,* respectively.

Using the simple perfusion-limited model to describe the time variation of the tissue pressure P as function of the tissue time constant τ, the tissue initial pressure P_I and the liquid back pressure P_B, we have:

$$(P - P_B)/(P_I - P_B) = e^{-t/\tau} \qquad (1)$$

where t is the time, s.

The gas pressure obtained from Fig. 3*a, b,* can be replotted on the semi-logarithmic plane $(P-P_B)/(P_I-P_B)-t$ as indicated in Fig. 4*a*.

Such a linear plot provides a means for determining the tissue time constant τ as it is equal to the reciprocal of the slope of the line correlating the dimensionless tissue pressure $(P-P_B)/(P_I-P_B)$ and the time t.

The time constant of the tissue perfused by water flow rate of 4.1 ml/s is shorter than that of the same tissue with water flow rate of 8.7 ml/s (Fig. 4*a*). For a particular dive condition (P_I) and a specific decompression stop (P_B), there is an optimal flow rate at which the elimination rate is maximum. For the particular conditions in Fig. 4*a*, this flow rate is 4.1 ml/s. Flow rates higher or lower than this optimal value will result in slower elimination rates.

Such a phenomenon is attributed mainly to the interaction between the gas bubbles and the perfusing stream. If the bubble wash-out process is not fast enough to carry the released bubbles away from the tissue, the liquid pressure increases which in turn results in an impairment of the elimination rate. At a high flow rate of 8.7 ml/s, the wash-out process is fairly fast in that it carries the released bubbles away from the tissue model almost as fast as they develop. Due to the large volume of these bubbles as well as the resistance of the liquid stream, the bubbles accumulate downstream raising the liquid pressure accordingly. This increase in the liquid pressure is followed by a consequent reduction in the elimination rate.

At high liquid flow rates, liquid pressure builds up slowly to a peak nearly equal to that developed at a lower flow rate. This is one of the reasons for impeding the elimination rate at higher flow rates.

Figure 4*b* shows the effect of varying the decompression stop, P_B, for a particular dive condition, P_I = 2 ATA, and water flow rate = 2.09 ml/s, on the tissue time constant. Surfacing to P_B = 1 ATA results in the fastest elimination rate among all of the considered decompression stops. Surfacing to P_B = 1.33 ATA, however, is found to produce a faster elimination than surfacing to a shallower stop at P_B = 1.17 ATA.

Figure 5*a* illustrates the effect of the initial tissue pressure and decompression stop on the tissue time constant. For the considered range of initial tissue pressures and for a liquid flow rate of 2.09 ml/s, elimination is fastest on decompression to P_B = 1 ATA and slowest if the decompression stop is at 1.66 ATA. Nonetheless, elimination is not always higher when the driving pressure difference is the largest. For example, if the initial tissue pressure is less than 2.46 ATA, then gas elimination is faster when

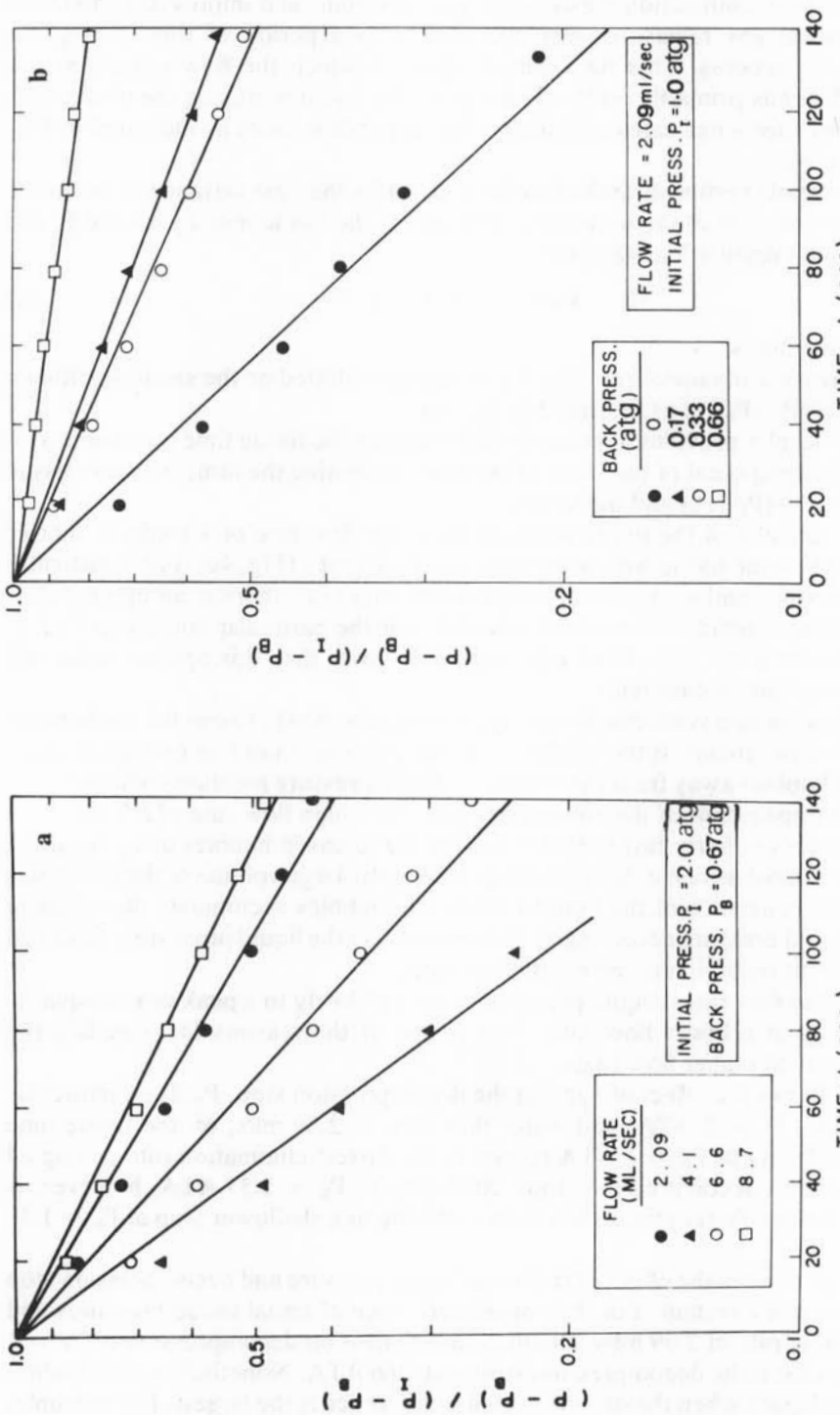

Fig. 4*a*: Dimensionless variation pattern of air pressure with time at different water flow rates with initial air pressure P_I = 3 ATA and the back pressure P_B = 1.66 ATA. *b*: Dimensionless variation pattern of air pressure with time at different back pressures with initial air pressure P_I = 2 ATA and water flow rate = 2.09 ml/s.

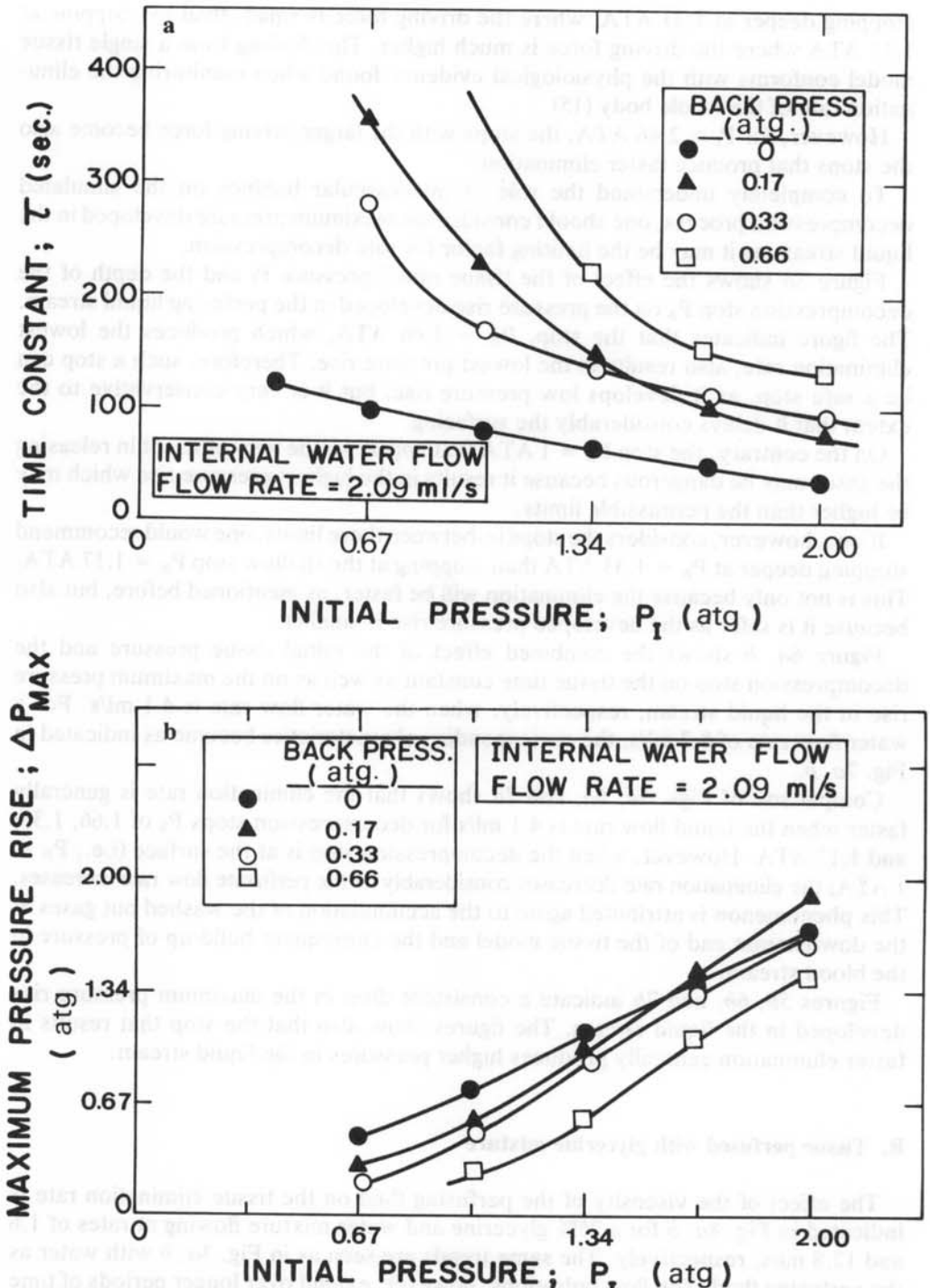

Fig. 5*a:* Effect of changing the initial pressure P_I and the back pressure P_B on the elimination time constant with water flow rate = 2.09 ml/s. *b:* Effect of changing the initial pressure P_I and the back pressure P_B on the maximum pressure rise with water flow rate = 2.09 ml/s.

stopping deeper at 1.33 ATA, where the driving force is small, than by stopping at 1.17 ATA where the driving force is much higher. This finding from a single tissue model conforms with the physiological evidence found when monitoring the elimination rate of the whole body (15).

However, for $P_I > 2.46$ ATA, the stops with the larger driving force become also the stops that produce faster elimination.

To completely understand the role of intravascular bubbles on the simulated decompression process, one should consider the maximum pressure developed in the liquid stream as it may be the limiting factor for safe decompression.

Figure 5*b* shows the effect of the tissue initial pressure P_I and the depth of the decompression stop P_B on the pressure rise developed in the perfusing liquid stream. The figure indicates that the stop, $P_B = 1.66$ ATA, which produces the lowest elimination rate, also results in the lowest pressure rise. Therefore, such a stop can be a safe stop, as it develops low pressure rise, but it is very conservative to the extent that it delays considerably the surfacing.

On the contrary, the stop $P_B = 1$ ATA that appears to be very efficient in releasing the gases may be dangerous because it results in the highest pressure rise which may be higher than the permissible limits.

If one, however, considers the stops in-between these limits, one would recommend stopping deeper at $P_B = 1.33$ ATA than stopping at the shallow stop $P_B = 1.17$ ATA. This is not only because the elimination will be faster, as mentioned before, but also because it is safer as the developed pressure rise is smaller.

Figure 6*a, b* shows the combined effect of the initial tissue pressure and the decompression stop on the tissue time constant as well as on the maximum pressure rise in the liquid stream, respectively, when the water flow rate is 4.1 ml/s. For a water flow rate of 8.7 ml/s, the corresponding characteristics become as indicated in Fig. 7*a, b*.

Comparison of Figs. 5*a*, 6*a*, and 7*a* shows that the elimination rate is generally faster when the liquid flow rate is 4.1 ml/s for decompression stops P_B of 1.66, 1.33, and 1.17 ATA. However, when the decompression stop is at the surface (i.e., $P_B = 1$ ATA) the elimination rate decreases considerably as the perfusate flow rate increases. This phenomenon is attributed again to the accumulation of the washed out gases at the downstream end of the tissue model and the consequent build-up of pressure in the blood stream.

Figures 5*b*, 6*b*, and 7*b* indicate a consistent drop in the maximum pressure rise developed in the liquid stream. The figures show also that the stop that results in faster elimination generally produces higher pressures in the liquid stream.

B. Tissue perfused with glycerine mixture

The effect of the viscosity of the perfusing fluid on the tissue elimination rate is indicated in Fig. 8*a, b* for a 25% glycerine and water mixture flowing at rates of 1.6 and 12.8 ml/s, respectively. The same trends are seen as in Fig. 3*a, b* with water as the perfusing fluid. The flow pulsations, however, extend over longer periods of time in the glycerine stream than in the water stream even at much higher flow rates. Furthermore, increasing the viscosity of the perfusing liquid is accompanied by a noticeable reduction in the rate of gas elimination.

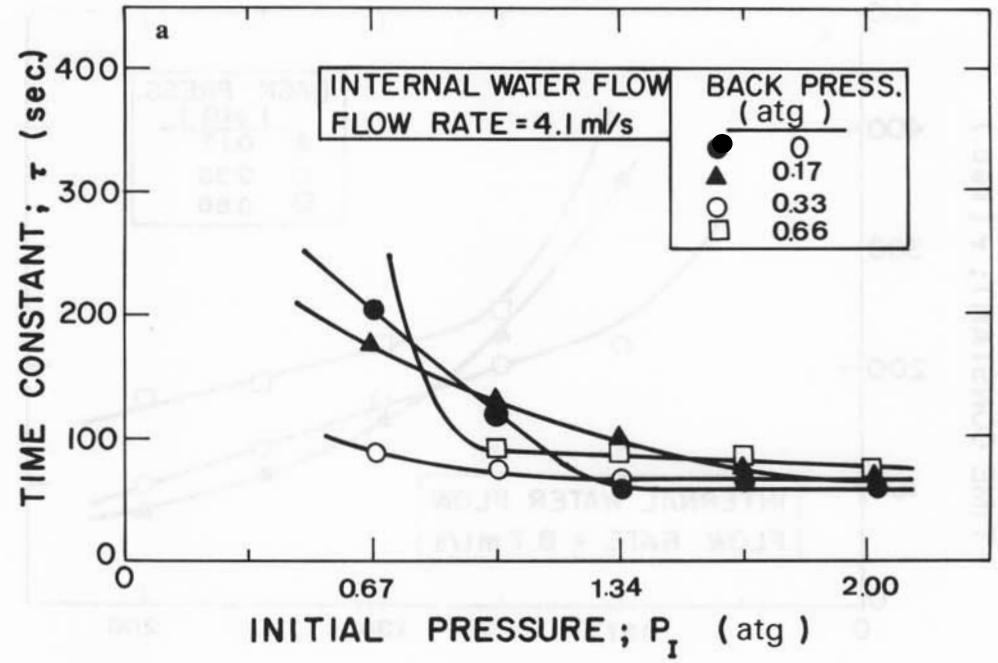

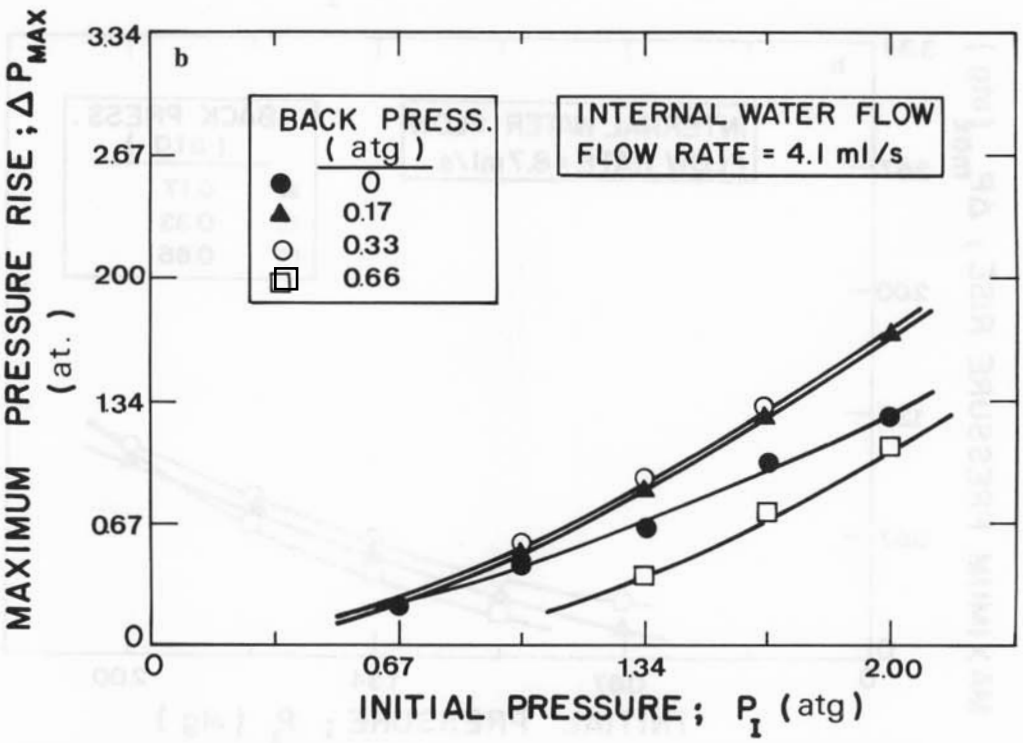

Fig. 6*a:* Effect of changing the initial pressure P_I and the back pressure P_B on the elimination time constant with water flow rate = 4.1 ml/s. *b:* Effect of changing the initial pressure P_I and the back pressure P_B on the maximum pressure rise with water flow rate = 4.1 ml/s.

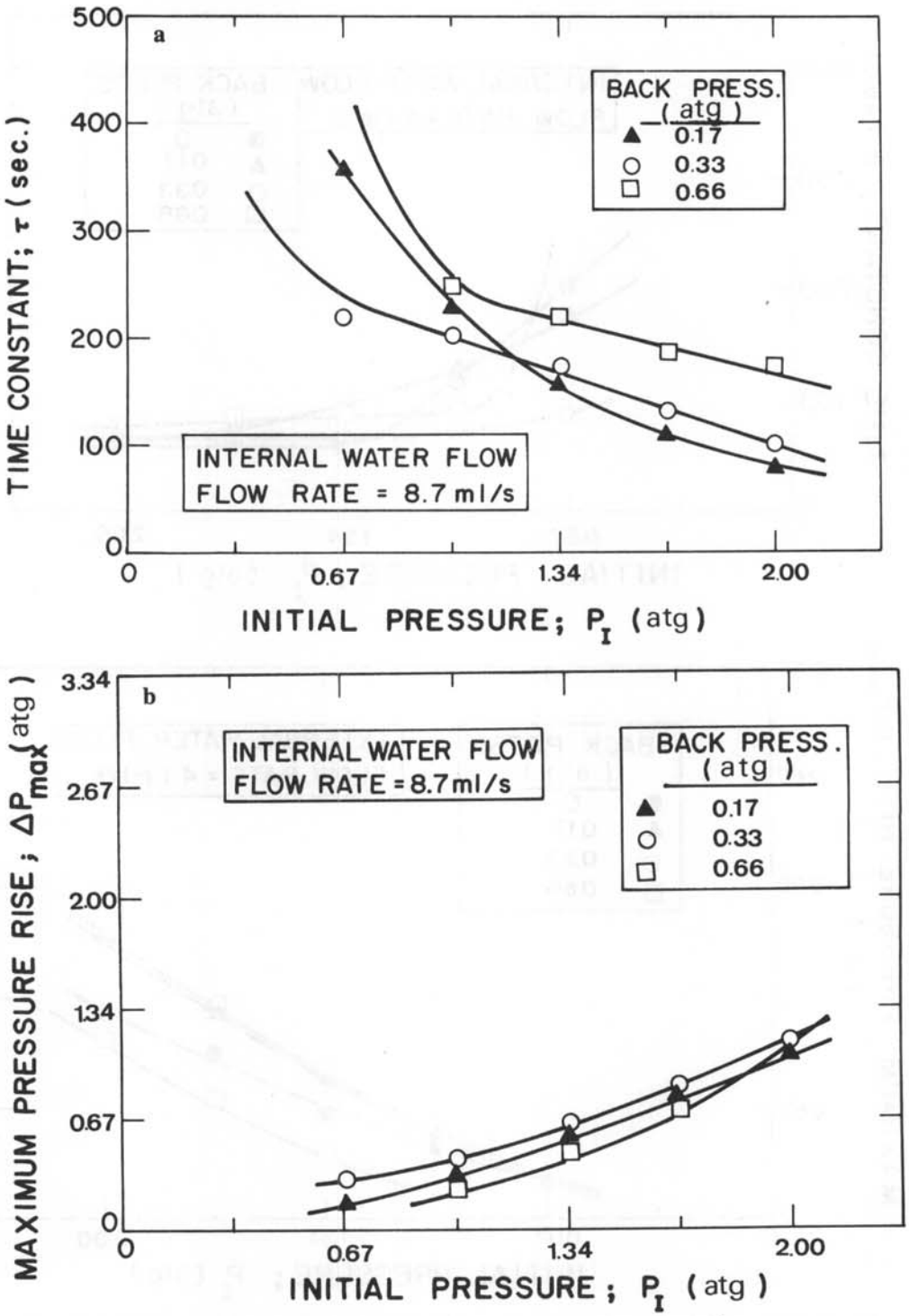

Fig. 7*a:* Effect of changing the initial pressure P_I and the back pressure P_B on the elimination time constant with water flow rate = 8.7 ml/s. *b:* Effect of changing the initial pressure P_I and the back pressure P_B on the maximum pressure rise with water flow rate = 8.7 ml/s.

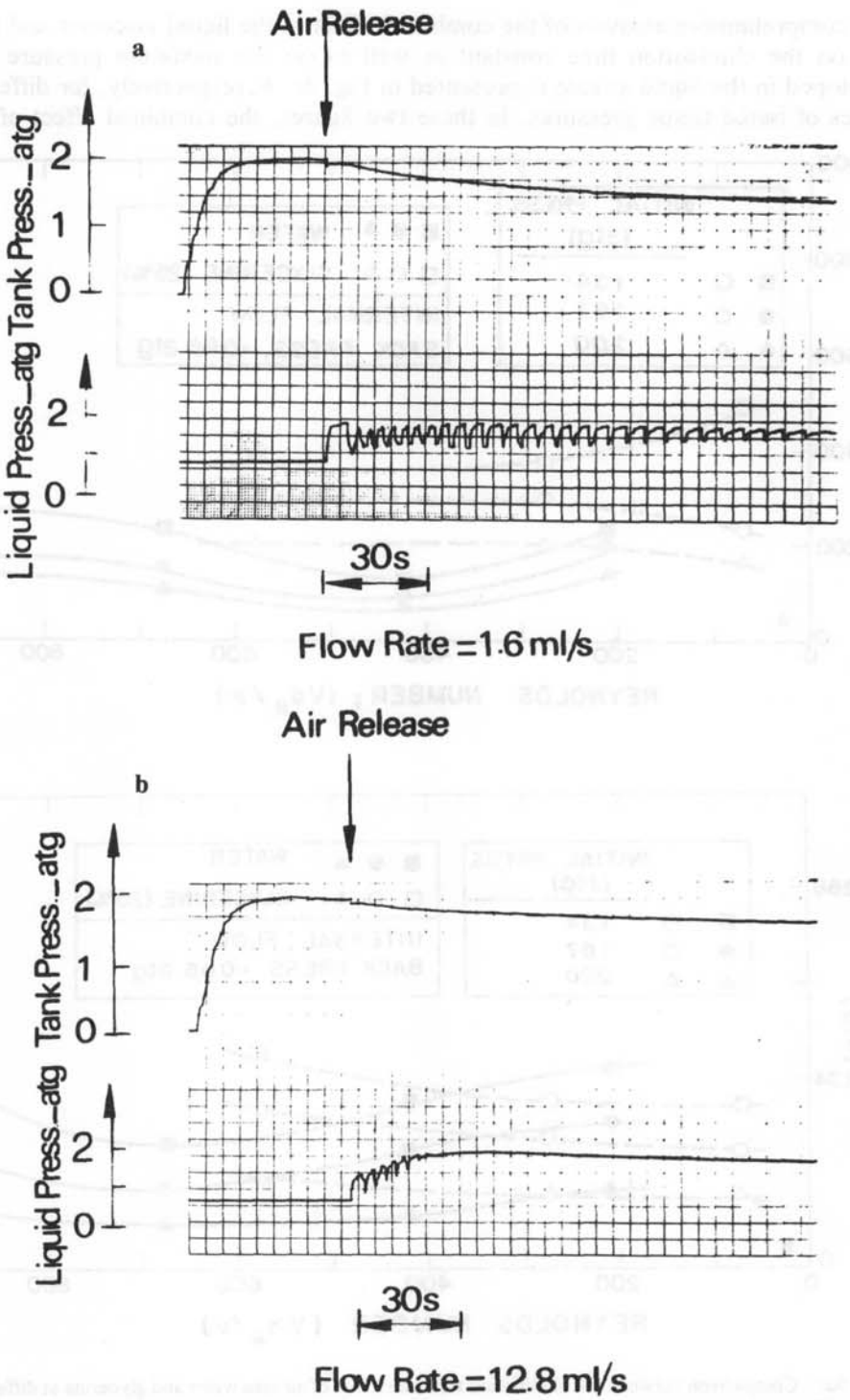

Fig. 8*a:* Time histories of air and glycerine pressure with initial air pressure P_I = 3 ATA, the back pressure P_B = 1.66 ATA and the glycerine flow rate = 1.6 ml/s. *b:* Time histories of air and glycerine pressure with initial air pressure P_I = 3 ATA, the back pressure P_B = 1.66 ATA and the glycerine flow rate = 12.8 ml/s.

A comprehensive analysis of the combined effect of the liquid viscosity and flow rate on the elimination time constant as well as on the maximum pressure rise developed in the liquid stream is presented in Fig. 9*a*, *b*, respectively, for different values of initial tissue pressures. In these two figures, the combined effect of the

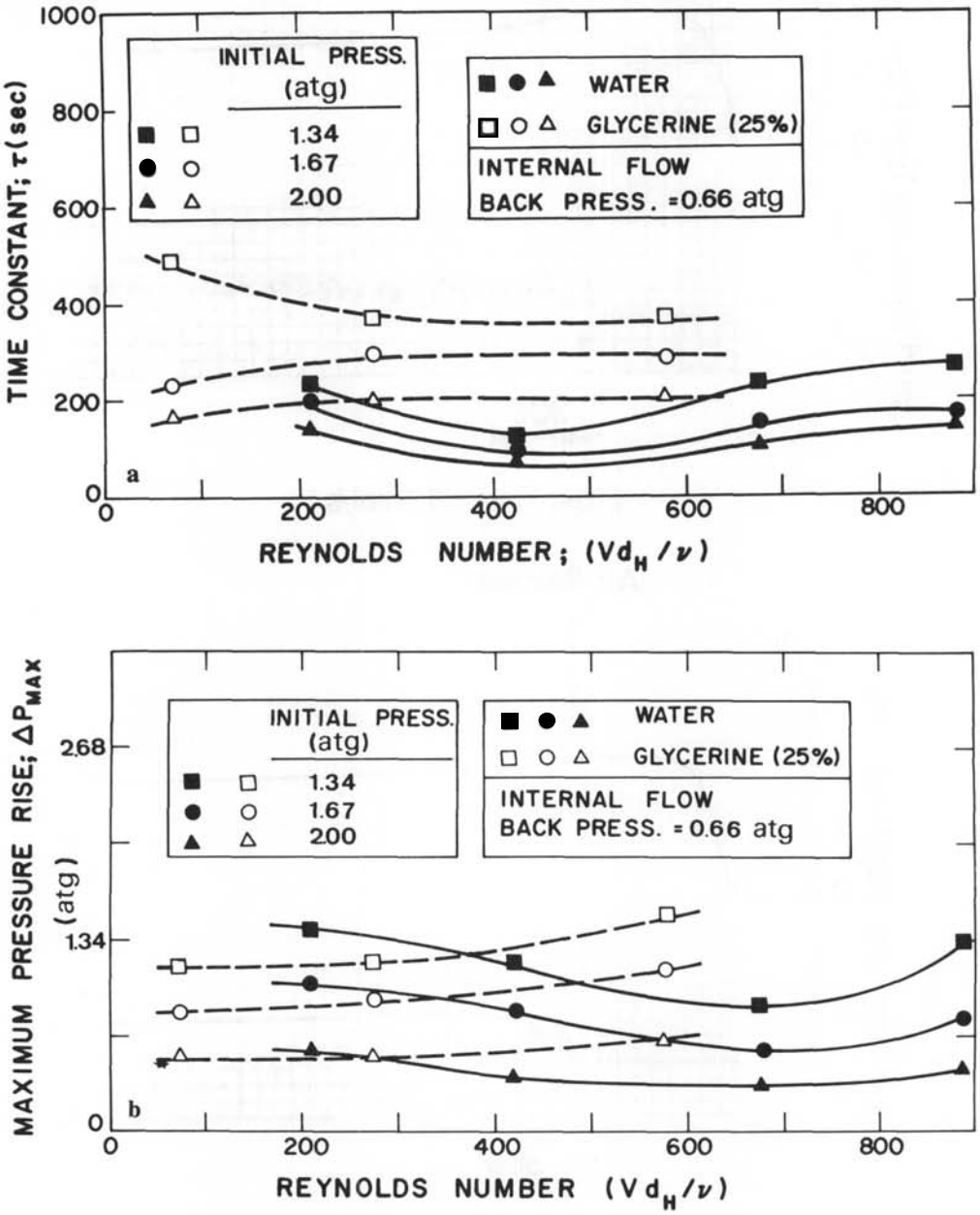

Fig. 9*a:* Comparison between the elimination time constants of air into water and glycerine at different values of Reynolds number and initial air pressure when the back pressure P_B = 1.66 ATA. *b:* Comparison between the maximum time pressure rise in water and glycerine at different values of Reynolds number and initial air pressure when the back pressure P_B = 1.66 ATA.

liquid kinematic viscosity υ and flow velocity V is described by the dimensionless Reynolds number R_N defined by:

$$R_N = V \cdot d_H / \upsilon \qquad (2)$$

where d_H is the inner diameter of the hollow cylindrical model of the tissue through which the liquid flows.

Figure 9*a* shows that, for the considered range of Reynolds number and for a particular level of initial tissue tension, the elimination rate is faster when the liquid perfusing the tissue is water. The glycerine mixture, being 2.25 times more viscous than the water, results in a considerable impairment of the elimination rate, particularly for values of Reynolds number higher than 200. Perfusing the tissue with the glycerine mixture results also in the development of pressures that are higher than those generated in the water stream as indicated in Fig. 9*b* for $R_N > 350$.

Accuracy of the results

Because the experiments were carried out on a mechanical analog of a tissue, it was possible to reproduce the results with reasonable accuracy which is only limited by the accuracy of measuring and interpreting the results. Repeating the tests at the extreme limits of the monitored parameters showed a peak variation in the tissue time constant of about $\pm$ 6 s.

CONCLUSIONS

This study has presented a qualitative analysis of the role of simulated intravascular bubbles in the gas elimination rates during the decompression process. The study utilized a porous-hollow cylindrical tissue model whose elimination time constant, for air, is found to vary between 0.5 and 7 min depending on the dive conditions and depth of decompression stop. Such wide variation in the time constant is attributed to the interaction between the developed intravascular bubbles, the liquid perfusing the tissue as well as the tissue itself. Emphasis should not be on the absolute value of the obtained time constants but rather on the general trends and phenomena associated with the intravascular release of bubbles. This is because the time constants can be increased by increasing the volume of the storage tank, for example, to obtain values that are comparable to those of fatty tissues.

Qualitative analysis of the results shows, however, that the originally steady liquid stream becomes pulsatile during decompression and the pressure pulsations extend for periods of time that depend on the liquid flow velocity and viscosity. High flow rates and low viscosity reduce the period of flow oscillation considerably. It is found also that, for particular initial tissue pressure and decompression stop, there is an optimal flow rate of the perfusing liquid at which the elimination rate is maximum. The experimental results indicate that there is an optimal decompression stop for each dive at which the gas elimination rate is maximum. Also, perfusion of the tissue with a high viscosity fluid impaired considerably the elimination rate.

Although the results show trends that parallel reported physiological evidence, one must point out that these trends should only be considered as qualitative in nature. This is due to the fact that the tested rigid and porous cylindrical model of the tissue

is too simple to simulate the complex geometry and flow conditions of a capillary-vein network.

For example, the rigid tissue model does not allow the formation or growth of extravascular gas bubbles although these bubbles have been considered by many investigators (3–6) to be a source of impairment of gas elimination. But the rigidity feature of the model was essential for studying the effect of intravascular bubbles alone. In actual decompression processes, the gas elimination will be influenced by the combined effects of intra- and extravascular bubbles.

Furthermore, the flow from the small diameter capillaries into the large diameter veins requires the inner diameter of the tissue model to be smaller than the tygon tubing draining it. But the tissue model is selected to have the opposite configuration in order to reflect the physiological condition that the total cross-sectional area of the capillary bed is larger than the cross-sections of the veins connected to it. The model has a ratio of capillary to vein cross-sectional areas of about 1.73 which is very close to the 1.91 ratio estimated for the human body (27). The considered range of Reynolds number is, however, higher than that encountered in the actual capillaries, mainly because of the practical physical dimensions of the model. These factors would therefore influence the actual rates of bubble washout in the human body during decompression and accordingly extrapolation of the observed results to the physiological systems would be invalid.

Extension of the work on a soft tissue model would be necessary for studying the combined effect of intra- and extravascular bubbles of air and other inert gases. Monitoring of the bubble formation and growth intra- and extravascularly will provide greater insight into the mechanism of decompression. Direct physiological monitoring techniques are essential to support quantitatively the phenomena reported here on the mechanical analog of the human tissue.

The study has, however, emphasized the role that intravascular bubbles have on the elimination rate during decompression.

Manuscript received for publication July 1983; revision received July 1985.

Baz A, Abdel-Khalik SI. Effet des bulles intravasculaires sur le débit de perfusat et les taux d'élimination des gaz après la décompression simulée d'un modèle tissulaire. Undersea Biomed Res 1986; 13(1):27–44.—Cette étude porte sur l'enregistrement des taux d'élimination des gaz d'un modèle cylindrique poreux de tissus humain durant des profiles simulés de décompression à simple palier. Les données suggèrent la présence d'un palier de décompression optimal pour chaque plongée auquel le taux d'élimination des gaz est maximum. L'effet produit par la variation de la vitesse de débit et la viscosité du liquide de perfusion du modèle tissulaire sur le taux d'élimination est déterminé pour différentes conditions de plongée. Même si cette étude a été effectuée sur un modèle tissulaire unitaire, elle offre un moyen pour expliquer certains phénomènes physiologiques observés dans les tissus humains.

bulles intravasculaires
taux optimal d'élimination
palier optimal de décompression

REFERENCES

1. Weathersby PK, Homer LD. Current concepts of inert gas exchange and decompression. In: Bachrach AJ, Matzen MM, eds. Underwater physiology VII. Proceedings of the seventh symposium on underwater physiology. Bethesda: Undersea Medical Society, 1981:687–698.

2. Buckles RG. The physics of bubble formation and growth. Aerosp Med 1968;39:1062–1069.
3. Albano G, Columba M. Gas nucleation concept applied to decompression. In: Lambertsen CJ, ed. Proceedings of the fourth symposium on underwater physiology. New York: Academic Press, 1971:193–204.
4. Yount DE, Strauss RH. Bubble formation in gelatin: a model for decompression sickness. J Appl Phys 1976;47:5081–5089.
5. D'Arrigo JS, Mano Y. Bubble production in agarose gels subjected to different decompression schedules. Undersea Biomed Res 1979;6:93–98.
6. Yount DE, Yeung CM, Kunkle TD. Some recent experiments on bubble formation in supersaturated gelatin. In: Bachrach AJ, Matzen MM, eds. Underwater physiology VII. Proceedings of the seventh symposium on underwater physiology. Bethesda: Undersea Medical Society, 1981:793–802.
7. Lightfoot EN, Baz A, Lanphier EH, Seireg AH. Role of bubble growth kinetics in decompression. In: Shilling CW, Beckett MW, eds. Underwater physiology VI. Proceedings of the sixth symposium on underwater physiology. Bethesda: Federation of American Societies for Experimental Biology, 1978:449–457.
8. Vann RD, Clark HG. Bubble growth and mechanical properties of tissue in decompression. Undersea Biomed Res 1975;2:185–194.
9. Hlastala M, Van Liew HD. Absorption of in-vivo inert gas bubbles. Respir Physiol 1975;24: 147–158.
10. Rosner DE, Epstein M. Effect of interface kinetics, capillarity and solute diffusion on bubble growth rates in highly saturated liquids. Chem Eng Sci 1972;27:69–86.
11. Tepper RS, Lightfoot EN, Baz A, Lanphier EH. Inert gas transport in the microcirculation: risk of isobaric supersaturation. J Appl Physiol 1979;46:1157–1163.
12. Hills BA. The alternating bubble theory of decompression. In: Berghage TE, ed. Proceedings of the seventh Undersea Medical Society Workshop. 1978:137–141.
13. Meisel S, Talmon Y, Kerem D. Evaluation of decompression tables by a model describing bubble dynamics in tissue. In: Bachrach AJ, Matzen MM, eds. Underwater physiology VII. Proceedings of the seventh symposium on underwater physiology. Bethesda: Undersea Medical Society, 1981:755–783.
14. Kindwall EP, Baz A, Lightfoot EN, Lanphier EH, Seireg AH. Nitrogen elimination in man during decompression. Undersea Biomed Res 1975;2:285–297.
15. Smith KH, Johanson DC. Hyperbaric decompression by means of bubble detection. Tech Rep NR 101-750. Washington, DC: Office of Naval Research, 1970.
16. Nishi RY, Kisman KE, Eatock BC, Buckingham IP, Masurel G. Assessment of decompression profiles and divers by Doppler ultrasonic monitoring. In: Bachrach AJ, Matzen MM, eds. Underwater physiology VII. Proceedings of the seventh symposium on underwater physiology. Bethesda: Undersea Medical Society, 1981:717–727.
17. Ackles KN, Korey A, Moschos M, McBurney LJ. The effect of repeated hyperbaric exposure on blood platelets in man. Undersea Biomed Res 1974;1:A21–22.
18. Bove AA, Famiano FC, Levin LL, Carey RA, Pierce AL, Lynch PR. Alterations in long-bone regional blood flow associated with inadequate decompression in dogs. Undersea Biomed Res 1977;4:169–182.
19. Hallenbeck JM, Bove AA, Elliott DH. Mechanisms underlying spinal cord damage in decompression sickness. Neurology 1975;25:308–316.
20. Krogh A. The number and distribution of capillaries in muscles with calculation of the oxygen pressure head necessary for supplying the tissue. J Physiol 1919;52:409–415.
21. Hennessy TR. Inert gas exchange in heterogeneous tissue, II, with perfusion. Math Biophys 1971;33:249–257.
22. Hennessy TR. The interaction of diffusion and perfusion in homogeneous tissue. Bull Math Biol 1974;36:505–526.
23. Matsen Corporation. Powder metallurgy engineering handbook, catalog No. 5MB Chicago, IL, 1983:13–21.
24. Haynes RH. The rheology of blood. Trans Soc Rheol 1961;5:85–101.
25. Ling SC, Atabek HB, Fry DL, Patel DJ, Janicki JS. Application of heated-film velocity and shear probes to hemodynamic studies. Circ Res 1968;23:789–801.

26. Adolfson J, Berghage TE. Perception and performance underwater. New York: John Wiley & Sons, 1974:175–204.
27. Wiederhielm CA. The capillaries, veins, and lymphatics. In: Ruch TC, Patton HD, eds. Physiology and biophysics II 20th ed. Circulation, respiration, and fluid balance. Philadelphia, PA: W. B. Saunders, 1974:129–145.